A Novel Image-Capturing Technique for the Experimental Study of Soil Deformations During Compaction

A novel image-capturing technique for the experimental study of soil deformations during compaction

C.T.S.Beckett (corresponding author)
School of Engineering and Computing Sciences,
Durham University,
Durham, DH1 3LE, UK
c.t.s.beckett@dur.ac.uk

C.E.Augarde
School of Engineering and Computing Sciences,
Durham University,
Durham, DH1 3LE, UK
charles.augarde@dur.ac.uk

Abstract

A method is described here for the monitoring of two layers of moist sandy-loam soil under compaction, where a flatbed scanner is used to capture large images of the deforming material. Particle Image Velocimetry (PIV) is used to track the movements of groups of particles within the soil. Due to their insufficient surface texture, PIV cannot be used on clayey soils. Therefore, to allow the analysis to take place, a novel use of a transparent clay is made whereby an artificial soil comprising transparent clay, sand and gravel is created to approximate the moist sandy loam soil. The design of a suitable compaction chamber and tests to determine optimal PIV parameters are discussed. The suitability and applicability of the use of a flatbed scanner are discussed and results are shown to confirm the success of the scanning method.

Keywords: Soil deformation, compaction, transparent clay, image analysis.

Introduction

Understanding the processes and causes of deformations in soils is important in a number of geotechnical applications and phenomena, for example: compaction (Ajaz and Parry, 1975; Tarantino and De Col, 2008; Tarantino, 2010); shearing (Jotisankasa et al., 2009; Hall et al., 2010); tunnelling (Take et al., 2005); installation of piles (White, 2002; Ni et al., 2010); and changes in water content (Wheeler and Sivakumar, 1995; Sivakumar and Wheeler, 2000; Sivakumar et al., 2006; Ferber et al., 2009; Gens, 2010). Such deformations are often difficult to monitor non-intrusively, although several advances have been made towards this goal. In the 1970s, Ajaz and Parry (1975) used lead shot target markers embedded in a regular pattern into the surface of a clay beam to evaluate bending strain in a compacting clay. The main drawback of the target marker method is, however, that the surface behaviour of the material is altered, so that the observed deformations can often not be representative of the unaltered specimen. In Love et al. (1987), photographs were used with small-scale laboratory models to track deformations of geogrid reinforcement placed at the base of a layer of granular fill on the surface of a soft clay. This technique relies on manually tracking areas of deforming material from one image to another and so is not suitable for large-scale or lengthy tests, where many images are required. More recently, Hall et al. (2010) used X-Ray micro Tomography (X-ray μCT) to observe deformations in a sand specimen subjected to a triaxial compression test. Although the use of X-ray μCT offers a truly non-intrusive test, the size of samples currently able to be tested using X-ray μCT machines are small (in the order of 20 cm^3), and tests are highly expensive, making parametric analyses unattractive. Popular scanning resolutions of roughly 0.2 mm (e.g. Udawatta et al., 2006; Kumar et al., 2010) also mean that small-scale influential soil properties, for example the microporosity (intra-aggregate pores, of the order of 1 to 100 μm, Udawatta et al. (2006); Zhang and Li (2010)), cannot be observed using this method.

An analysis of existing techniques for deformation analysis shows that there is a need for techniques that can offer both quantitative and qualitative monitoring of deformations for use with medium-scale laboratory samples. These techniques need to be inexpensive to run in order to encourage parametric testing.

Image Analysis

Image analysis techniques in geotechnical engineering are a family of methods which allow deformations of large specimens to be observed and recorded non-intrusively (Lee and Bassett, 2006; Zhang et al., 2006). Particle Image Velocimetry ("PIV", also known as "digital image correlation" (Pan et al., 2009; Liu and Iskander, 2010)) is an example of a growing geotechnical image analysis technique whereby the motion of particles or collections of particles in a deforming medium are tracked by comparing digital images of that medium taken over several time intervals. PIV evolved from Laser Doppler Velocimetry (LDV), developed for use with fluid mechanics, where laser pulses are used to illuminate seed particles in a moving fluid at set time intervals. Assuming that the particles are travelling with the fluid, the fluid flow pattern at the location of the seed particle can then be evaluated (Adrian, 1986, 1991).

In PIV, a digital image of a deforming material is divided into "test patches" of pixels, and these are compared with corresponding (larger) "search patches" in a subsequent image after a known time interval. The location at which the highest correlation between the test and search patches is found indicates the displaced position of the patch such that full-field displacements and strains can then be determined (Adrian, 1991; White et al., 2003; Meguid et al., 2008; Pan et al., 2009) (Figure 1). The use of a patch of pixels creates a greater range of pixel intensities when compared to individual pixels which improves the match to that patch in the second image (White et al., 2003; Pan et al., 2009).

PIV has been extended to use with geotechnical materials and has been successful in measuring particle and void size distributions and the movement and rotations of soil particles behind transparent viewing screens (Bhatia and Soliman, 1990; Guler et al., 1999; Zhang et al., 2006), in tracking large numbers of disc-shaped particles in order to approximate granular flow (Paikowski and Xi, 2000) and in larger applications recording the displacements of a range geogrid soil reinforcement products under tensile loading (Shinoda and Bathurst, 2004). In contrast to fluids or gases, intrusive markers often are not required for soils since the soil grains themselves serve as tracers (Slominski et al., 2007). Unlike in fluid mechanics, where each seed particle is interrogated individually (Adrian, 1986), the centroidal movement of the test patch between the two images is taken to be the average movement for all of the particles within that patch. Centroidal movement

to sub-pixel accuracy can be calculated using iterative spatial domain cross-correlation– or peak-finding fitting algorithms (to name two popular methods), with the former being the fastest and most accurate but the latter being the simplest (White, 2002; White et al., 2003; Zhang et al., 2006; Pan et al., 2009).

The accuracy of PIV depends on the quality of the image and the number of pixels used per test patch: the greater the number of pixels, the lower the error in finding the best match in the subsequent image but the longer the analysis time per patch (White, 2002; Pan et al., 2009). The disadvantage of using larger test patches is that fewer patches can be overlain on a given image, reducing the analysis resolution. Tracking accuracy is also affected by the magnitude of the displacements: if the displacement is an integer number of pixels, then the accuracy is increased, as less emphasis is placed on the fitting algorithm (White et al., 2003). In fluid flow analyses, particles are tracked using an illuminated plane (the plane of the photograph). Particle displacements out-of-plane to the illuminated plane are therefore not recorded, which can lead to spurious results. A similar problem arises if particles move out-of-plane to the sampling window in geotechnical analyses. Three-dimensional 'digital volume correlation" techniques can be used for tracking the three-dimensional displacements of particles in a solid volume, however 3-D methods will not be commented on here (Pan et al., 2009). PIV cannot be used to track large displacements as the patterns within the test patches as well as their locations will change (Slominski et al., 2007). Increasing the size of the search patch to accommodate larger deformations can also lead to multiple false matches for the test patch within the search limits, as well as increasing analysis time (White, 2002). PIV cannot be used effectively on clayey materials due to their lack of surface definition. The surface of a clayey material can be modified, for example by embedding target markers as used in Ajaz and Parry (1975), however this will affect the resulting deformations and so cannot be considered a non-intrusive test (White, 2002; White et al., 2005). A textured flock was sprinkled over the surface of a kaolin clay in Teh et al. (2008) in order to monitor its displacements, following recommendations made in White (2002) and White et al. (2005); however, the flock can adhere to both the deforming material and the viewing screen, such that its movements are no longer representative of the deformations taking place (White, 2002).

A grid of control markers, placed over the viewing screen or object of interest, is used in order to transform "image-space" displacements (in pixels) into "object-space" displacements (in mil-

limetres or equivalent). These markers do not move with respect to the boundary of the deforming material, so that tracking of the control markers allows any movement of the capturing device to be eliminated: this is particularly important in geotechnical centrifuge modelling, where the motion of the centrifuge will cause a camera boom or arm to deflect, leading to an apparent movement of particles in an un-corrected image (White, 2002). Image distortion must be considered when converting between image– and object-space coordinates. This had previously been achieved by using a single scaling factor, however this is only valid if the camera obeys the pinhole model where the object plane is parallel to the image plane and the pixels on the camera's CCD (Charged Couple Device) are square (White et al., 2003). Examples of corrections that are required include: non-coplanarity of image and object planes; lens distortion (radial and tangential); pixel non-squareness; and refraction through the viewing window. In total, sixteen additional numerical image correcting parameters were identified by White (2002) to accurately convert between image- and object-space coordinates.

Here we demonstrate the use of a flatbed scanner to capture images of a soil as it deforms during compaction. The scanner offers a number of advantages for use with PIV when compared to a digital camera. Firstly, the image size produced by a scanner is far larger; a modest flatbed scanner can achieve scans of 1200dpi, resulting in an A4-sized image (11.7×8.3 inches) of roughly 140 megapixels. The latest generation commercial digital camera offers 21 Megapixels (model reference: Canon EOS-1Ds Mark III, correct at time of writing). Another advantage is the ability to select a scanning resolution without having to consider and accurately measure the distance between the image source and the viewing screen is also a significant advantage. Secondly, the plane of the scanned image is guaranteed to be parallel to the viewing screen, as the scanner's scanning glass can be placed in direct contact with the viewing screen. This not only eliminates non-coplanarity corrections, but also removes the need to consider refraction through the viewing window, as the scanning axis of the scanning bar remains perpendicular to the viewing window as the scan is taken. Thirdly, the cost of the equipment is significantly reduced: whereas a current generation digital camera could cost in the region of £4500 (model reference: Canon EOS-1Ds Mark III, correct at time of writing), a suitable flatbed scanner can cost as little as £25.

An apparent disadvantage of the scanner over the camera is the time required to capture the image; however, as long as no deformation occurs during the scanning process, this is not an issue.

Another disadvantage is the set viewing screen size: whereas a digital camera could capture a greater viewing area at a sacrifice of resolution (pixels/mm) by being moved away from the image plane, the scanner must remain in contact with the viewing screen. Therefore, the scanner is only suitable for tests that can fit within the scanning window. A scanner would therefore not be suitable for capturing fast-moving or large deformation processes, for example that occur in fluid or granular flow, but is excellently suited to the intermittent displacement that occurs in soils during operations such as compaction as long as the sample size is representative.

Development of the Test Procedure

Compacted Earthen Materials

The impetus for the development of this procedure is the ongoing research into earthen construction materials at Durham University. An experiment was devised to observe the deformations of two layers of soil, one above the other, on compaction, as part of a larger investigation of the compacted earthen building material "rammed earth" (RE) which is seeking to identify its geotechnical and structural properties and to link its microstructure to the method of formation. RE is a form of unbaked earthen construction where walls are constructed from moist layers of sandy-loamy subsoil (between 100 and 150 mm deep (Walker et al., 2005)) placed between formwork and compacted. The formwork is removed after compaction in order to allow the structure to dry, a process through which the material gains most of its strength (Betts and Miller, 1937; Jaquin et al., 2008, 2009).

Design of the Compaction Chamber

The compaction chamber was designed to accommodate multiple layers of soil so that deformations on compaction could be observed. A sketch of the compaction chamber showing principal dimensions is shown in Figure 2, and a photograph of the chamber with scanner fitted is shown in Figure 3. The chamber's viewing window is limited to the size of the flatbed scanner, in this case to an area of 300 mm×250 mm or just larger than an A4 piece of paper. This size allows for two layers of soil of 150 mm depth to be placed in the chamber and compacted (the final compacted depth being less than 100 mm on average for RE-suitable soils). The width of 300 mm is also representative of an internal or non-load bearing RE wall (Houben and Guillaud, 1996; King, 1996;

Walker et al., 2005; Easton, 2007). The chamber is 100 mm wide to allow for a sufficiently-large rammer. Two 10 mm thick Perspex panels form the front and rear of the chamber to allow the deforming material to be viewed. Two 15 mm thick steel panels form the chamber sides to prevent bulging. A 2.5kg "flat head" rammer is mounted above the chamber: its position can be changed by means of the rammer carriage and guide rails. The rammer is sufficiently long so that the drop height can be set to 300 mm above the surface of the soil for each strike. This is to comply with the Light Proctor Test, chosen as the authors believe that it more closely approximates the conditions that would exist within the soil in a full-scale wall on construction. Two clamps mounted on the front of the chamber hold the scanner in place, in contact with the front panel.

Development of "Artificial Rammed Earth"

As mentioned above, PIV cannot usually be used on clayey soils due to insufficient surface texture. In this study, rather than use the established techniques of tracking deformations in clayey materials using embedded target markers or texturing the surface with flock (Ajaz and Parry, 1975; Teh et al., 2008), which are unsuitable due to the large deformations on compaction, it was decided to substitute the clay in the RE for an artificial, transparent medium. Transparent media can be used to model granular and clayey soils, depending on the application. In the former case, grains of a given refractive index are placed in a container and saturated with a fluid of the same refractive index (Allersma, 1982; Siemens et al., 2010). In the latter case, amorphous silica (or "fumed silica") is mixed with a fluid of the same refractive index to form a solid, jelly-like clay substitute (Iskander et al., 2002; McKelvey et al., 2004; Liu and Iskander, 2010). Iskander et al. (2002) found that the transparent material used in their tests had geotechnical properties that were consistent with a wide range of natural clays. The material used in McKelvey et al. (2004) ("Trinity College Dublin" or "TCD" material) had geotechnical properties consistent with normally consolidated alluvial clays. Transparent materials offer a much safer method to monitor the deformations of structures in soils in the laboratory than other non-intrusive methods, for example radiography (Hughes and Withers, 1974). Furthermore, as testing is relatively quick and inexpensive, parametric analysis becomes more attractive.

In this work, the TCD material was combined with sand and pea gravel in the ratio of 5:4:1 (TCD:sand:pea gravel, by mass) in order to approximate a clayey RE soil. These ratios were chosen

according to work done by Hall and Djerbib (2004) and represent a high clay-content RE soil as specified by the "CRATerre" institute (Houben and Guillaud, 1996). The TCD was not required to be transparent due to its being mixed with non-transparent materials. Therefore, extensive testing to produce a truly transparent material was not required. Instead, the TCD produced here was translucent, which was sufficient for use in this experiment. The resulting combined material was dubbed "Artificial Rammed Earth" (ARE).

Parametric Analyses

A series of preliminary tests was carried out to ensure that the scanned images would be adequate for PIV analysis, using a mixture of sands. A scanning resolution of 600 dpi was selected, producing a 35 megapixel image over an A4 size. The resulting images were sufficiently detailed to allow for accurate PIV analysis but not so large as to require too great a computational effort, determined using sample test patch sizes of 128×128 pixels at a central spacing of 128 pixels (i.e. the patches are in contact without overlapping) and the software "geoPIV", developed by Prof. Dave White. geoPIV was used to perform all subsequent PIV analyses.

At 600 dpi, a sand grain of 2 mm average diameter would be represented by a bounding box of roughly 47×47 pixels, such that a test patch of 128×128 pixels would represent roughly 9 such grains. In the original work by White (2002), errors in displacement tracking for a number of materials were determined using a nominal resolution of 0.1 mm/pixel, such that the same sand grain would only occupy a bounding box of 20×20 pixels. The resulting empirical relationship between patch size and the error in displacement tracking (in pixels) is given by (White et al., 2003) as

$$\rho_{pixel} = \frac{0.6}{L} + \frac{150000}{L^8}. \tag{1}$$

resulting in errors of 0.03 pixels for the 20 pixel bounding box and 0.01 pixels for the 47 pixel bounding box, or a threefold increase in accuracy for the 600 dpi setting.

Further tests were carried out to determine the optimum size (in pixels) for the test patches. Test patch sizes of 64×64 pixels at 64 pixel centres, 128×128 pixels at 128 pixel centres and 256×256 pixels at 256 pixel centres were considered. Results showed that test patches of 128×128 pixels produced the clearest data in an acceptable analysis time. It was found that the more-dense test patch

mesh produced too many vectors for the displacement field to be legible, whilst the less dense mesh did not produce a sufficiently detailed displacement field. As geoPIV uses the Fast Fourier Transform method in order to determine the centroidal displacement of patches, it is recommended that patches should be of size 2^n pixels (where n is an integer) to reduce computational time (White, 2002). Therefore, no further patch sizes were investigated.

The "search boundary" is a border of pixels placed around the test patch to determine the size of the search patch (and so the maximum displacement that can be recorded). Search boundary limits of 10, 30 and 50 pixels were tested with combinations of the above patch sizes: a 50 pixel boundary produced too many wild vectors, whilst a 10 pixel boundary could not adequately track particle displacements. 30 pixels was therefore selected as a compromise, creating a corresponding maximum displacement for tracking of roughly 1.8 mm (roughly 1.3 mm vertically or horizontally) at 600 dpi with a precision of 0.06 mm. Unlike the requirement for test patches to be 2^n pixels in size, no such restriction exists for the search patch, as only a test patch sized part of the search patch is interrogated to determine the correlation.

Control markers were placed at known intervals on the surface of the viewing screen (the front Perspex panel). As image distortion is negated by having the scanning glass in contact and parallel with the viewing screen, only four control markers, placed at the four corners of the viewing window, were required. This represents an advantage over the methods used by White (2002), White et al. (2003) and Iskander et al. (2002) as the control marker grid obscures as little of the deforming material as possible.

Results and Discussion

Compaction testing was conducted by placing a level, 110 mm deep layer of ARE material into the compaction chamber. A scan of the un-compacted material was taken to act as a starting point for the PIV analysis prior to compaction. The ARE was compacted by moving the rammer from the right of the chamber to the left in 50 mm intervals and then reversing the direction until a constant compacted level was achieved. A scan of the deformed material was taken after each strike of the rammer, once the rammed had been retracted. A second 110 mm deep layer of ARE material was then added on top of the first and the process of scanning and compacting repeated.

The average compacted depths of the first and second layers were 67.1 mm and 73.7 mm respectively, corresponding to a 39% and 33% compaction (by volume): this is a favourable comparison to the expected compaction of an actual RE layer, which is roughly 33% (Walker et al., 2005), indicating that the ARE material is comparable to an actual RE soil for compaction testing.

Examples of results for the PIV analysis of the scanned images are shown in Figures 4-6: the displacement vectors show the centroidal movement of the test patches, scaled by a factor of five, such that a 'dot' represents no movement. The image behind the displacement field shows the material after compaction, i.e. the new particle positions. The axes show the size of the scanning window in millimetres (note that the units on the ordinate axis are inverted, as pixels are numbered from the top left corner of the image: displacements have been corrected for this). Figures 4 and 5 show the displacements after two strikes of the rammer, whilst Figure 6 shows particle displacements after eleven strikes (i.e. the first strike after two complete passes over the top of the material have been made). Deformation fields calculated from the captured PIV data corresponding to Figures 4 to 6 are shown in Figures 7 to 9 respectively. As can be seen in Figures 4 to 9, compaction results in significant deformation underneath and around the rammer face, as expected. As this deformation is large (i.e. greater than 1.8 mm, the additional size of the search patch) the displacement vectors in these regions are untrustworthy: their purpose is only to indicate those regions where deformations are the largest. Of interest is the apparent particle flow away from these regions into the more undisturbed material, showing that the action of compaction causes considerable horizontal as well as vertical deformations, which may or may not be advantageous given the desired application.

The top of the first ARE layer is clearly visible in Figures 5 and 6 as a dark band running across the material at roughly 180 mm from the top of the silo. It can be seen that the already-compacted material is not affected by the compaction of an overlying layer. A comparison of Figures 7 and 8 shows a very similar pattern for the deformations of the first and second layers, again suggesting that the first layer is acting as incompressible with respect to the second layer. Figures 8 and 9 also confirm the lack of deformations in the region occupied by the first ARE layer. This is an important result in terms of RE construction, as it suggests that the material properties of each layer are determined by compaction of that layer alone, and are not dependent on other layers in the structure. For a more detailed analysis of the experimental results and the performance of the ARE material the reader is referred to Beckett and Augarde (2010).

As the scanner is set to have a zero focal length (i.e. set to focus on items that are in contact with the scanning glass) the images of the deformed material are blurred. The separating of the scanner and the deforming material by the viewing screen is necessary to avoid scratching the scanning glass, which would lead to erroneous PIV results. However, as the separation distance is constant (the scanner is not moved during the test), it can be assumed that the effect of blurring is also constant both along the length of the image (as the scanning bar traverses the scanning glass rather than capturing the entire image from one location) and for the duration of the test. The effect of blurring should therefore not influence particle tracking, as long as sufficient particle definition is maintained; the illuminated scanning bar should be enough to ensure this. The larger test patch size afforded by the use of the scanner also serves to reduce the impact of blurring due to more pixels being matched between images. If a focused image is desired, then the front panel can be reduced in thickness; however, if it is made too thin then it will bulge on compaction which might not only cause damage to the scanner but will also result in a non-constant focal length, such that focusing effects will need to be considered when determining the final deformations.

Conclusion

A new procedure has been described for the non-intrusive monitoring of soil deformations *in situ*. The procedure develops the use of image analysis and PIV for geotechnical materials making novel use of a flatbed scanner. The procedure and experiment are considerably cheaper than other non-intrusive testing methods currently available. Tests on the compaction of an artificial rammed earth material demonstrate the potential of the procedure, particularly for qualitative analysis of soil deformations. It is anticipated this idea could be employed to study a number of other geotechnical problems in the future.

Acknowledgements

The authors would like to thank Prof. David White (UWA) for providing the software "geoPIV" and for his help in its use. The authors would also like to thank Mr. Rob Stow (Durham Tees Valley Airport) for providing the raw materials required for TCD manufacture. The author is funded by a studentship awarded by the School of Engineering and Computing Sciences, Durham University.

References

Adrian, R., 1986. Multi-point optical measurements of simultaneous vectors in unsteady flow–a review. International Journal of Heat and Fluid Flow 7 (2), 127–145.

Adrian, R. J., 1991. Particle imaging techniques for experimental fluid mechanics. Annual Review of Fluid Mechanics 23, 261–304.

Ajaz, A., Parry, R. H. G., 1975. Stress-strain behaviour of two compacted clays in tension and compression. Géotechnique 25 (3), 495–512.

Allersma, H., 1982. Photo-elastic stress analysis and strains in simple shear. In: Vermeer, P. A., Luger, H. J. (Eds.), Proc., IUTAM Symposium on Deformation and Failure of Granular Materials. A. A. Balkema, Rotterdam, pp. 345–353.

Beckett, C. T. S., Augarde, C. E., September 2010. Development of microstructure in compacted earthen building materials. In: Alonso, E., Gens, A. (Eds.), Unsaturated Soils. Fifth International Conference on Unsaturated Soils, CRC Press, pp. 139–144.

Betts, M. C., Miller, T. A. H., 1937. Rammed earth walls for buildings. Farmer's Bulletin 1500.

Bhatia, S. K., Soliman, A. F., 1990. Frequency distribution of void ratio of granular materials determined by an image analyzer. Soils and Foundations 30 (1), 1–16.

Easton, D., 2007. The Rammed Earth House, completely revised edition Edition. Chelsea Green Publication Company, Vermont (USA).

Ferber, V., Auriol, J. C., Cui, Y. J., Magnan, J. P., 2009. On the swelling potential of compacted high plasticity clays. Engineering Geology 104 (3-4), 200–210.

Gens, A., 2010. Soil-environment interactions in geotechnical engineering. Géotechnique 60 (1), 3–74.

Guler, M., Edil, T. B., Bosscher, P. J., 1999. Measurement of particle movement in granular soils using image analysis. Journal of Computing in Civil Engineering 13 (2), 116–122.

Hall, M., Djerbib, Y., 2004. Rammed earth sample production: context, recommendations and consistency. Construction and Building Materials 18 (4), 281–286.

Hall, S. A., Bornert, M., Desrues, J., Pannier, Y., Lenoir, N., Viggiani, G., Bésuelle, P., 2010. Discrete and continuum analysis of localised deformation in sand using x-ray μct and volumetric digital image correlation. Géotechnique 60 (5), 315–322.

Houben, H., Guillaud, H., 1996. Earth construction - a comprehensive guide., second ed. Edition. Intermediate Technology Publications, London (UK).

Hughes, J. M. O., Withers, N. J., 1974. Reinforcing of soft cohesive soils with stone columns. Ground Engineering 3, 42–49.

Iskander, M. G., Liu, J., Sadek, S., 2002. Transparent amorphous silica to model clay. Journal of Geotechnical and Geoenvironmental Engineering 128 (3), 262–273.

Jaquin, P. A., Augarde, C. E., Gallipoli, D., Toll, D. G., 2009. The strength of unstabilised rammed earth materials. Géotechnique 59 (5), 487–490.

Jaquin, P. A., Augarde, C. E., Legrand, L., Jul 2008. Unsaturated characteristics of rammed earth. In: First European Conference on Unsaturated Soils. Toll, D. G., Durham, England, pp. 417–422.

Jotisankasa, A., Coopy, M., Ridley, A., Jun 2009. The mechanical behaviour of an unsaturated compacted silty clay. Géotechnique 59 (5), 415–428.

King, B., 1996. Buildings of Earth and Straw: Structural Design for Rammed Earth and Straw-Bale Architecture. Ecological Design Press, California (USA).

Kumar, S., Anderson, S., Udawatta, R., Gantzer, C., May 2010. Ct-measured macropores as affected by agroforestry and grass buffers for grazed pasture systems. Agroforestry Systems 79 (1), 59–65.

Lee, Y., Bassett, R., Jan. 2006. Application of a photogrammetric technique to a model tunnel. Tunnelling and Underground Space Technology 21 (1), 79–95.

Liu, J., Iskander, M. G., 2010. Modelling capacity of transparent soil. Canadian Geotechnical Journal 47, 451–460.

Love, J. P., Burd, H. J., Miligan, G. W. E., Houlsby, G. T., 1987. Analytical and model studies of reinforcement of a layer of granular fill on a soft clay subgrade. Canadian Geotechnical Journal 24 (4), 611–622.

McKelvey, D., Sivakumar, V., Bell, A., Graham, J., Jul 2004. Modelling vibrated stone columns in soft clay. Proceedings of the Institution of Civil Engineers-Geotechnical Engineering 157 (3), 137–149.

Meguid, M., Saada, O., Nunes, M., Mattar, J., Mar. 2008. Physical modeling of tunnels in soft ground: A review. Tunnelling and Underground Space Technology 23 (2), 185–198.

Ni, Q., Hird, C., Guymer, I., 2010. Physical modelling of pile penetration in clay using transparent soil and particle image velocimetry. Géotechnique 60 (2), 121–132.

Paikowski, G., Xi, F., 2000. Particle motion tracking utilizing a high- resolution digital CCD camera. Geotechnical Testing Journal 23 (1), 123–134.

Pan, B., Qian, K., Xie, H., Asundi, A., 2009. Two-dimensional digital image correlation for in-plane displacements and strain measurement: A review. Measurement Science and Technology 20, 062001.

Shinoda, M., Bathurst, R. J., 2004. Strain Measurement of Geogrids using a Video-Extensometer Technique. Geotechnical Testing Journal 27 (5), 8p.

Siemens, G., Peters, S., Take, W. A., 2010. Analysis of a drawdown test displaying the use of transparent soil in unsaturated flow applications. In: Alonso, E., Gens, A. (Eds.), Unsaturated Soils. Fifth International Conference on Unsaturated Soils, CRC Press.

Sivakumar, V., Tan, W. C., Murray, E. J., McKinley, J. D., Feb 2006. Wetting, drying and compression characteristics of compacted clay. Géotechnique 56 (1), 57–62.

Sivakumar, V., Wheeler, S., 2000. Influence of compaction procedure on the mechanical behaviour of an unsaturated compacted clay. part 1: Wetting and isotropic compression. Géotechnique 50 (4), 359–368.

Slominski, C., Niedostatkiewicz, M., Tejchman, J., Apr. 2007. Application of particle image velocimetry (piv) for deformation measurement during granular silo flow. Powder Technology 173 (1), 1–18.

Take, W. A., White, D. J., Bowers, K. H., Moss, N. A., Jun 15-17 2005. Remote real-time monitoring of tunnelling-induced settlement using image analysis. In: Bakker, K. J., Bezuijen, A., Broere, W., Kwast, E. A. (Eds.), 5th International Conference on Getechnical Aspects of Underground Construction in Soft Ground. Taylor & Francis Ltd, Amsterdam, pp. 771–777.

Tarantino, A., September 2010. Unsaturated soils: compaction versus reconstituted states. In: Alonso, E., Gens, A. (Eds.), Unsaturated soils. Fifth International Confernce on Unsaturated Soils, CRC Press, pp. 113–136.

Tarantino, A., De Col, E., 2008. Compaction behaviour of clay. Géotechnique 58 (3), 199–213.

Teh, K. L., Cassidy, M. J., Leung, C. F., Chow, Y. K., Randolph, M. F., Quah, C. K., Dec 2008. Revealing the bearing capacity mechanisms of a penetrating spudcan through sand overlying clay. Géotechnique 58 (10), 793–804.

Udawatta, R. P., Anderson, S. H., Gantzer, C. J., Garrett, H. E., Aug. 2006. Agroforestry and grass buffer influence on macropore characteristics: A computed tomography analysis. Soil Sci Soc Am J 70 (5), 1763–1773.

Walker, P., Keable, R., Martin, J., Maniatidis, V., 2005. Rammed Earth: Design and Construction Guidelines. BRE Bookshop, Watford (UK).

Wheeler, S., Sivakumar, V., 1995. An elasto-plastic critical state framework for unsaturated soils. Géotechnique 45 (1), 35–53.

White, D. J., 2002. An investigation into the behaviour of pressed-in piles. Thesis, University of Cambridge, Cambridge.

White, D. J., Randolph, M. F., Thompson, B., 2005. An image-based deformation measurement system for the geotechnical centrifuge. International Journal of Physical Modelling in Geotechnics 5 (3), 1–12.

White, D. J., Take, W. A., Bolton, M. D., Sep 2003. Soil deformation measurement using particle image velocimetry (PIV) and photogrammetry. Géotechnique 53 (7), 619–631.

Zhang, G., Liang, D. F., Zhang, J. M., 2006. Image analysis measurement of soil particle movement during a soil-structure interface test. Computers and Geotechnics 33 (4-5), 248–259.

Zhang, L. M., Li, X., Oct. 2010. Microporosity structure of coarse granular soils. J. Geotech. and Geoenvir. Engrg. 136 (10), 1425–1436.

Figure 1: Image manipulation during PIV analysis, after White et al. (2003)

Figure 2: Sketch of the compaction chamber, showing principal dimensions in mm.

Figure 3: Photograph of the compaction chamber with scanner in place. Principal dimensions are shown in Figure 3.

Figure 4: Initial particle displacements after two strikes (scaled by a factor of 5 with the rammer striking between 200 and 300 mm in the silo length dimension) during compaction of the first ARE layer (units in mm).

Figure 5: Initial particle displacements after two strikes (scaled by a factor of 5 with the rammer striking between 200 and 300 mm in the silo length dimension) during compaction of the second ARE layer (units in mm).

Figure 6: Particle displacements after 11 strikes (scaled by a factor of 5 with the rammer striking between 200 and 300 mm in the silo length dimension) half way through the compaction of the second ARE layer (units in mm).

Figure 7: Contour plot of initial particle displacements after two strikes (with the rammer striking between 200 and 300 mm in the silo length dimension) during the compaction of the first ARE layer (units in mm).

Figure 8: Contour plot of initial particle displacements after two strikes (with the rammer striking between 200 and 300 mm in the silo length dimension) during the compaction of the second ARE layer (units in mm).

Figure 9: Contour plot of particle displacements after 11 strikes (with the rammer striking between 200 and 300 mm in the silo length dimension) during the compaction of the second ARE layer (units in mm).

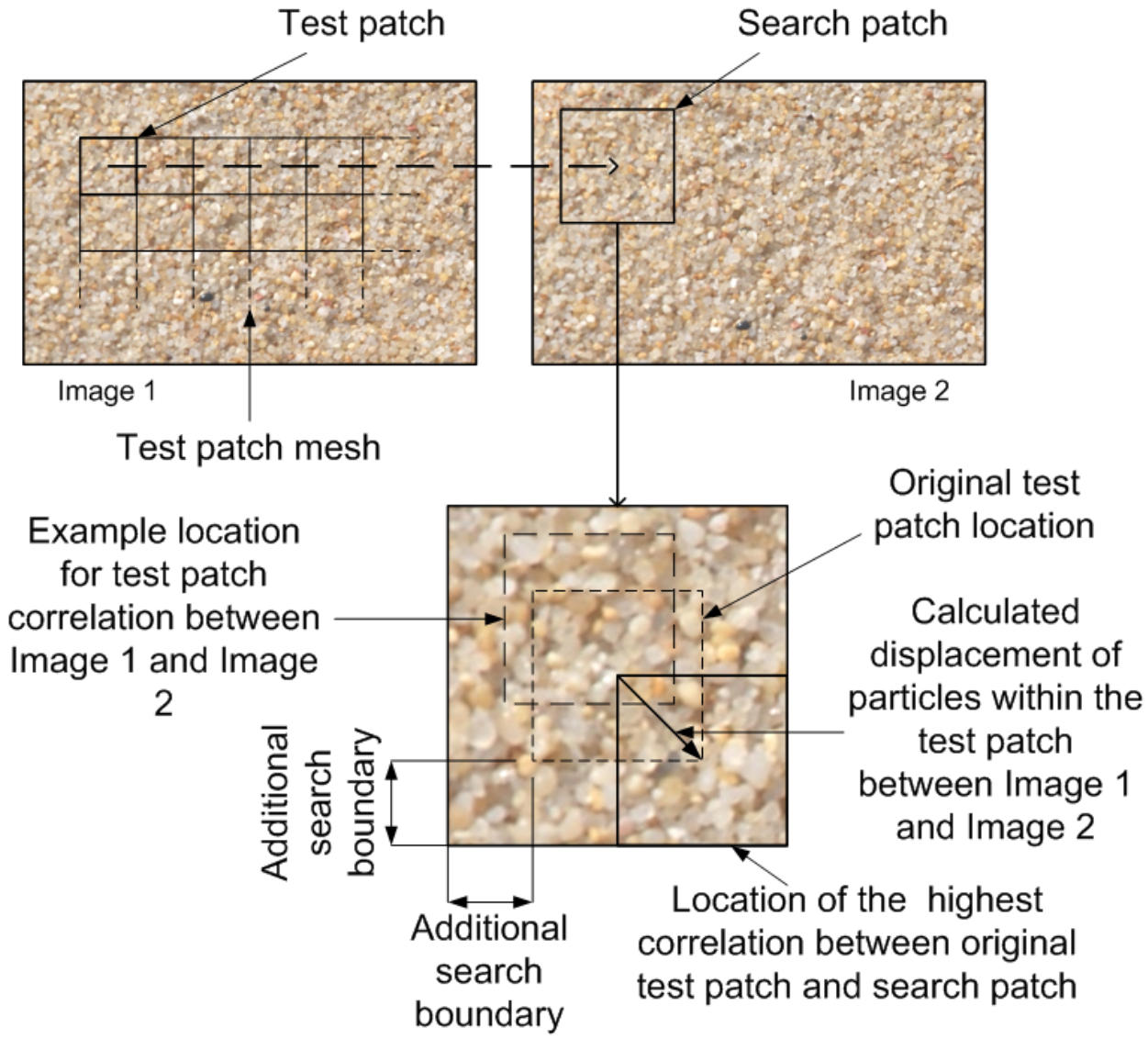

Figure 1: Image manipulation during PIV analysis, after White et al. (2003)

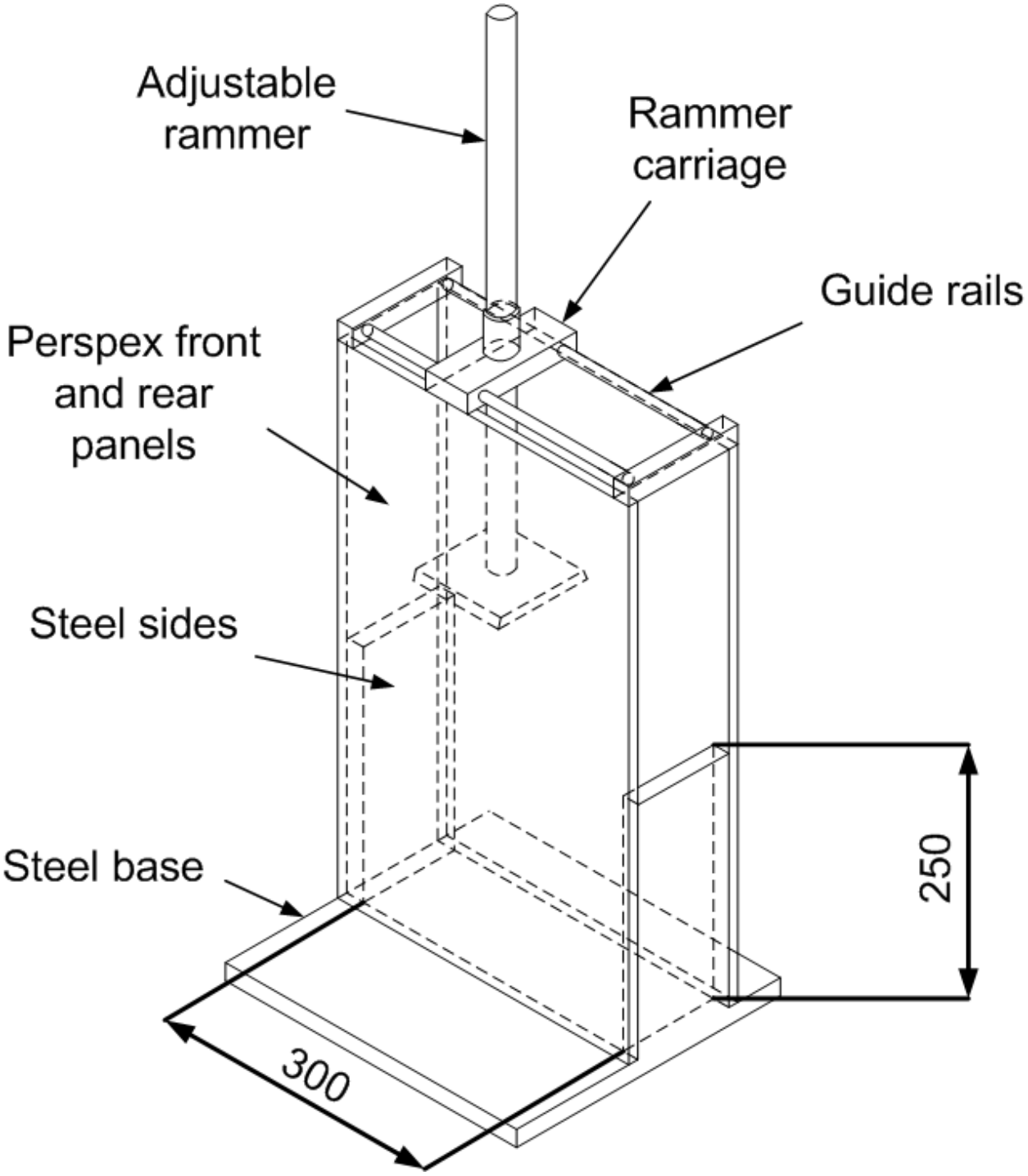

Figure 2: Sketch of the compaction chamber, showing principal dimensions in mm.

Figure 3: Photograph of the compaction chamber with scanner in place. Principal dimensions are shown in Figure 2.

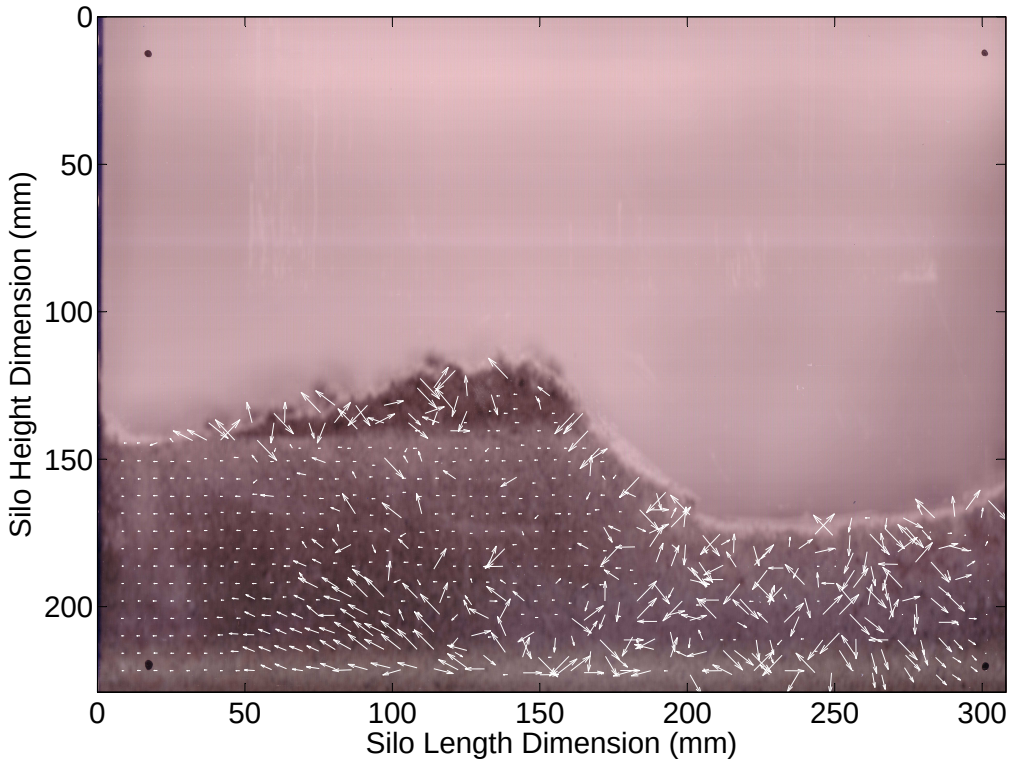

Figure 4: Initial particle displacements after two strikes (scaled by a factor of 5 with the rammer striking between 200 and 300 mm in the silo length dimension) during compaction of the first ARE layer (units in mm)

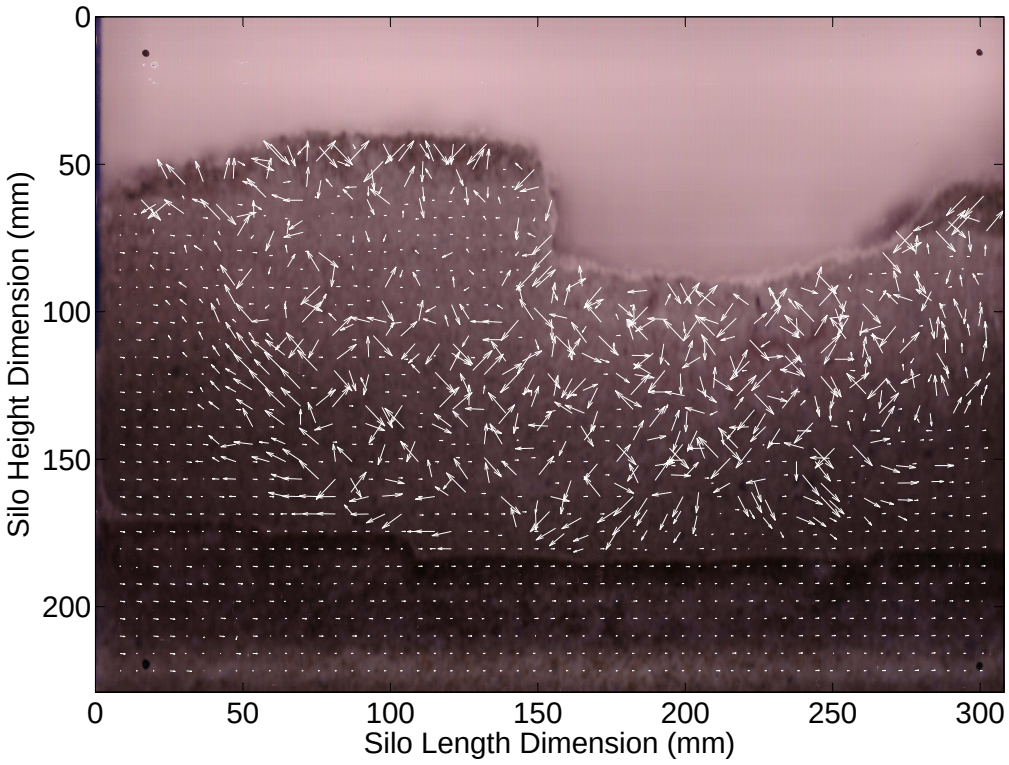

Figure 5: Initial particle displacements after two strikes (scaled by a factor of 5 with the rammer striking between 200 and 300 mm in the silo length dimension) during compaction of the second ARE layer (units in mm).

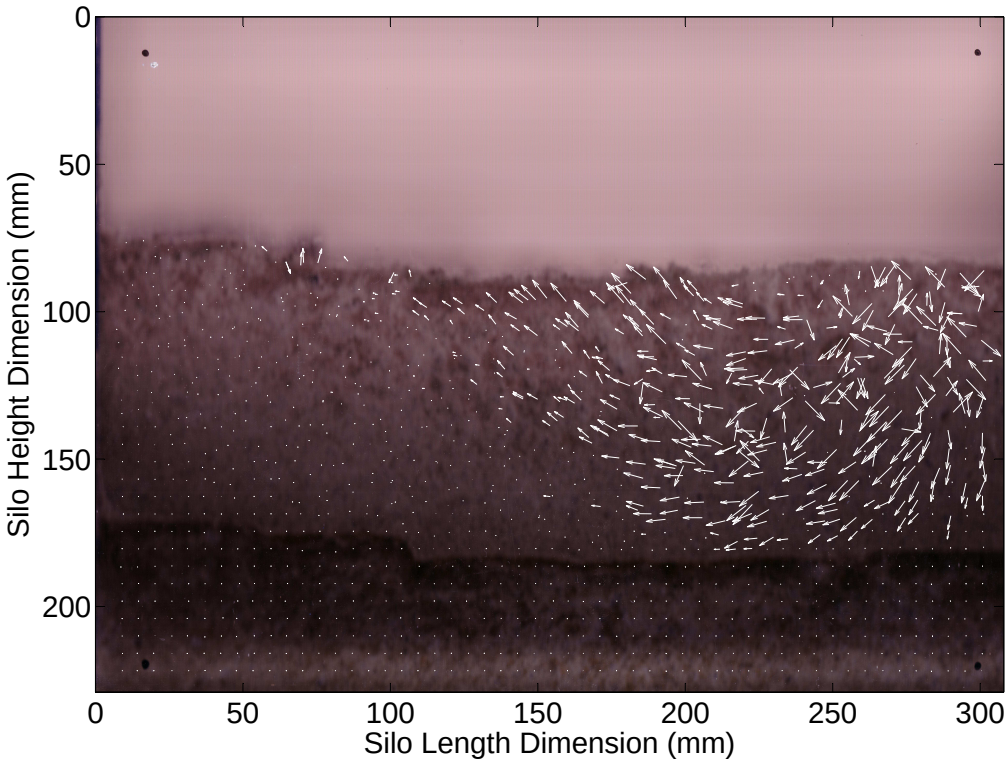

Figure 6: Particle displacements after 11 strikes (scaled by a factor of 5 with the rammer striking between 200 and 300 mm in the silo length dimension) half way through the compaction of the second ARE layer (units in mm).

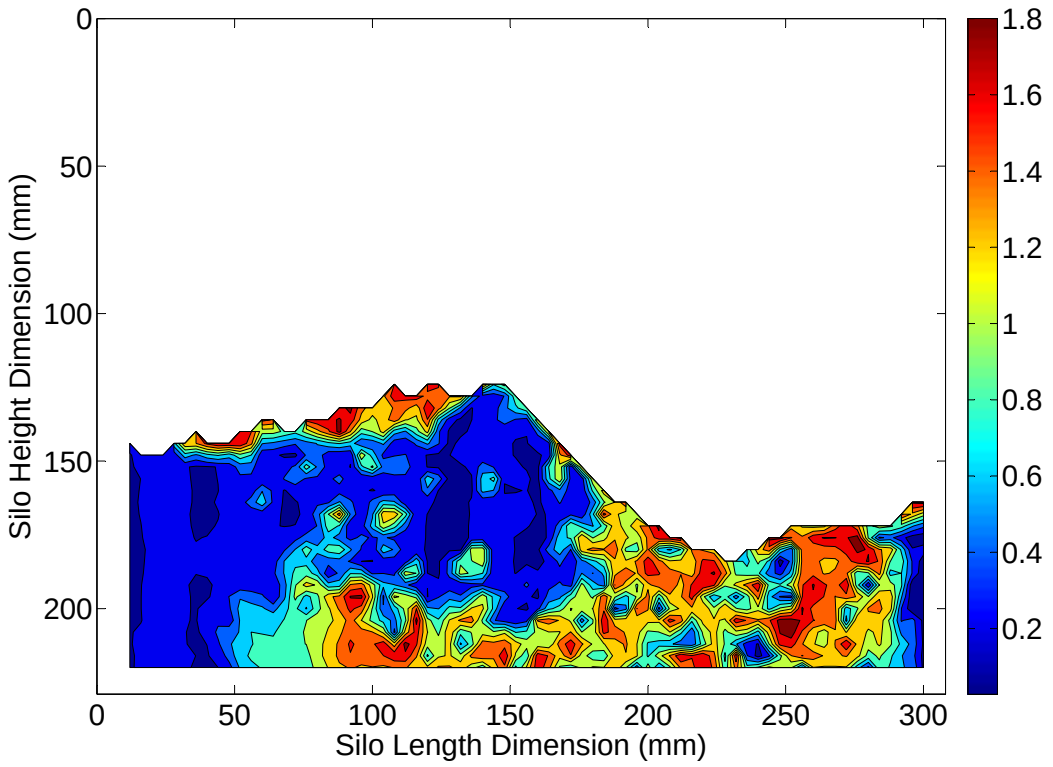

Figure 7: Contour plot of initial particle displacements after two strikes (with the rammer striking between 200 and 300 mm in the silo length dimension) during the compaction of the first ARE layer (units in mm).

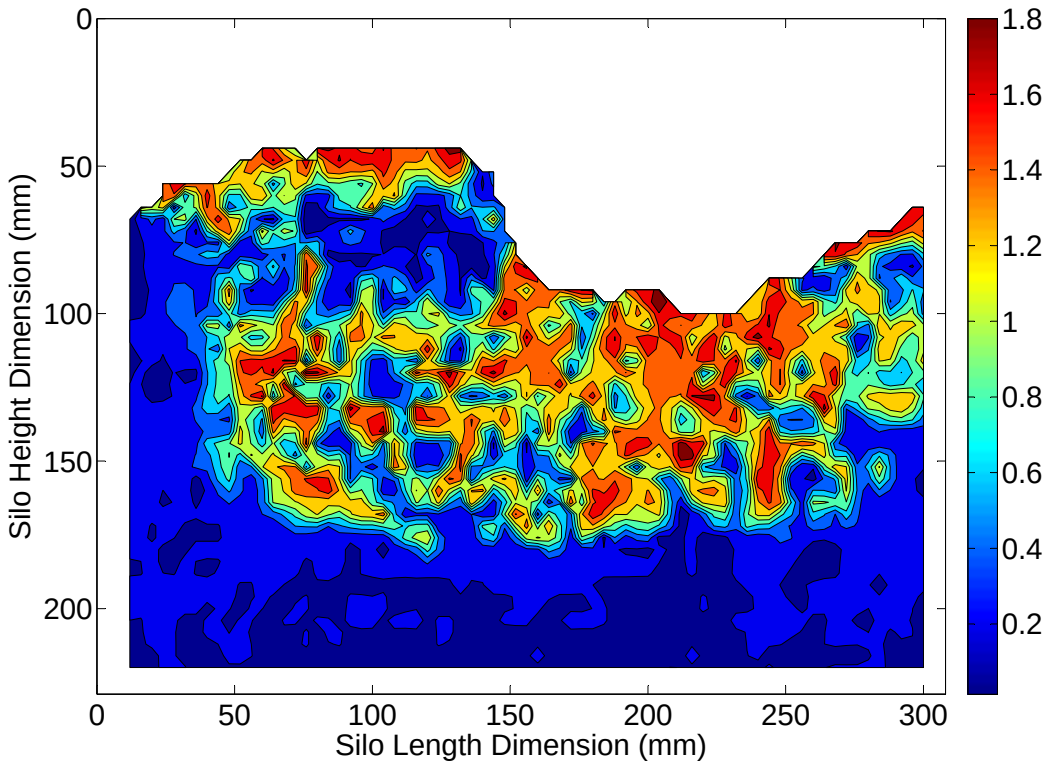

Figure 8: Contour plot of initial particle displacements after two strikes (with the rammer striking between 200 and 300 mm in the silo length dimension) during the compaction of the second ARE layer (units in mm).

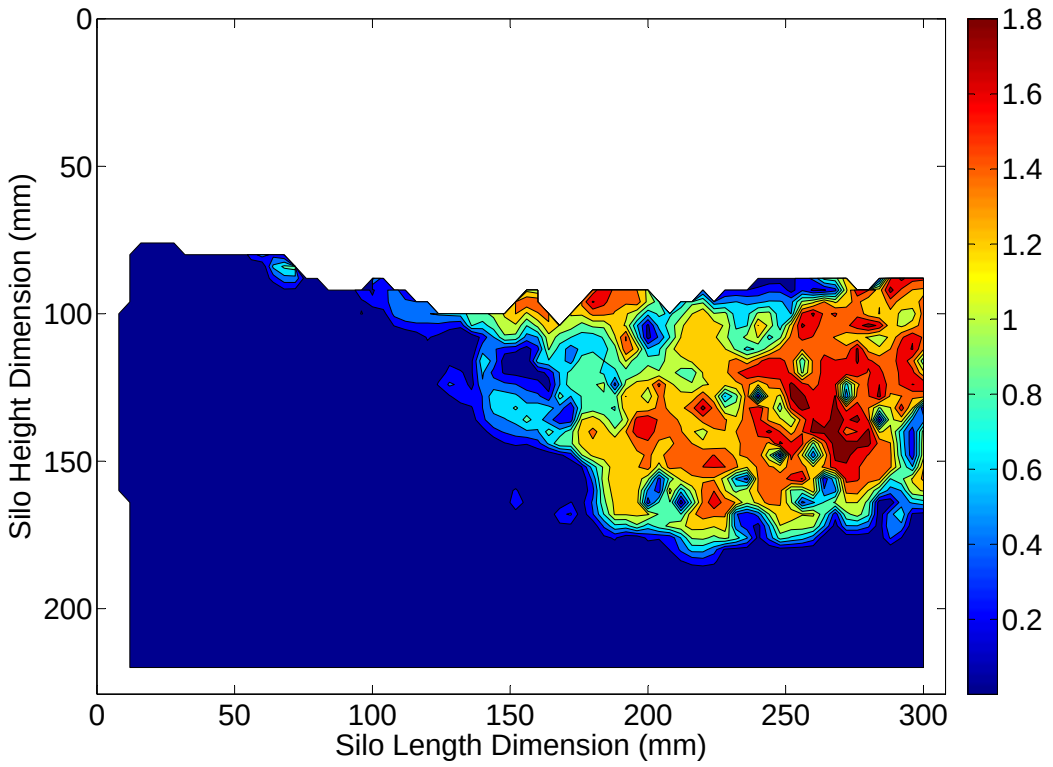

Figure 9: Contour plot of particle displacements after 11 strikes (with the rammer striking between 200 and 300 mm in the silo length dimension) during the compaction of the second ARE layer (units in mm).